EARTHQUAKE ENGINEERING AND STRUCTURAL DYNAMICS, VOL. 26, 815–838 (1997)

VARIABLE GAIN FEEDBACK CONTROL TECHNIQUE OF ACTIVE MASS DAMPER AND ITS APPLICATION TO HYBRID STRUCTURAL CONTROL

ICHIRO NAGASHIMA[1]* AND YUZO SHINOZAKI[2]

[1]*Technology Research Center, Taisei Corporation, Nasemachi, Totsuka-ku Yokohama 245, Japan*
[2]*Department of Architecture and Environmental Design, Kyoto University, Sakyo-ku, Kyoto 606, Japan*

SUMMARY

A systematic design procedure and an algorithm are devised for variable gain feedback (VGF) control of buildings with active mass damper (AMD) systems. The limit of the stroke length of the auxiliary mass, which is considered to be one of the most important physical constraints for application of AMD systems to actual structures, is studied. A set of variable feedback gains is designed as a function of a single variable that indicates a trade-off between the reduction of the building response and the amplitude of the auxiliary mass stroke, and this variable is on-line controlled to keep the amplitude of the auxiliary mass stroke constant, and within its limits.

A design method of static output feedback controller for modal control of buildings with non-classical damping is also presented. Next, an efficient control method for hybrid structural control is developed, with combined use of the VGF control and the static output feedback control. It is shown through numerical examples that the proposed control method effectively adapts the control performance according to the variation in the intensity level of the external excitations in such a manner that the amplitude of the auxiliary mass stroke is kept within its limits and the control power is restrained as well. The application range of the AMD systems is thereby improved significantly. © 1997 by John Wiley & Sons, Ltd.

Earthquake Engng. Struct. Dyn., **26**, 815–838 (1997)

No. of Figures: 15. No. of Tables: 1. No. of References: 30.

KEY WORDS: active mass damper; limit of stroke length; variable gain feedback; static output feedback; LQ optimal control

1. INTRODUCTION

The active structural control has been investigated and utilized in various applications throughout the last several decades and application to civil engineering structures started in mid-1980s.[1] A number of applications have already been found mostly in Japan.[2] Several types of active control systems have been developed, including active tendon, variable stiffness, active mass damper, etc.; among these, the AMD system has proved to be the most popular in actual applications. In Japan, many types of AMD systems for active structural control of tall buildings and bridge towers have been developed in order to improve their habitability against wind and earthquake excitations.[3–7] A feedback control with constant feedback gains designed by linear control theories such as direct velocity feedback, LQ optimal control or H^∞ controls, are usually adopted.

One of the important problems concerning the application of the linear control theories to the AMD systems is the lack of adaptivity to the variation in the intensity level of the external excitations, i.e. for stronger excitations, the control performance deteriorates and sometimes even the whole system should be stopped because of the physical limits imposed by the stroke length, the control power or the control force;

* Correspondence to: Ichiro Nagashima, Technology Research Center, Taisei Corporation, 344-1 Nasemachi, Totsuka-ku, Yokohama 245, Japan

CCC 0098–8847/97/080815–24$17·50

Received 23 August 1996
Revised 6 February 1997

for weaker excitations, on the other hand, the capacity of the system cannot be fully utilized. Among the physical limits of the AMD systems, the limit on control force, which is a control variable itself, is rather easy to deal with and therefore has been investigated by several researchers.

One way to design controllers with bounded control forces would be to solve optimal control problems; for example, the time optimal control problem and the minimum energy problem. These optimal control problems usually lead to two-point boundary value problems, for which open-loop bang-bang solutions are obtained. An optimal bang-bang control with quadratic performance index was investigated by Wonham[8] and its application has been recently attempted to control response of a building with an AMD system[9,10]. Although these optimal control problems have been solved in principle, open-loop solutions are difficult to calculate or the resulting switching surfaces are complicated to work with. In addition, control chattering due to high-frequency switching of the control force often occurs. For these reasons, in most applications, the optimal control solution has not been used so far.

Among other design techniques that consider the control force limit, bang-bang control methods based on the Lynapunov equation[11] are often attempted. Kelly *et al.*[12] applied this type of control method to active control of base isolated buildings. Application to AMD systems has also been studied.[13,14] However, the problem with these control techniques is that the solutions tend to be unnecessarily conservative compared to the optimal bang-bang solution and, consequently, the control performance of closed-loop systems may suffer. In addition, undesirable control chattering due to high-frequency switching of the control force often occurs and great care should also be taken for spillover instability at higher models.[15]

As for the AMD systems, even when the control force is limited by applying the control techniques mentioned above, the amplitude of the auxiliary mass stroke and the required control power would increase with the intensity level of the external excitations. Therefore, it is not sufficient to consider the constraint on the control force alone. The stroke length of the auxiliary mass as well as the control power are more critical constraints for actual applications than the control force, because of the practical limitations on the cost, space and electric power supplement available for the AMD systems. In addition, the control force saturation is allowable to some extent: for example, it is well known that LQ optimal control has gain margin not less than $\frac{1}{2}$, which means that even if the generated control force is 50 per cent less than the required control force, control instability does not occur. On the contrary, once the amplitude of the auxiliary mass stroke reaches its limits, the whole system should be stopped in order to avoid damage to the system itself as well as the building structure. Thus, a control algorithm which can handle the limits of the stroke length of the auxiliary mass as well as the control power has to be developed to improve the application range and reliability of the AMD systems in actual applications.

Variable gain feedback (VGF) control is a practical technique that enables one to consider the limits of both the control force and the auxiliary mass stroke. This control method usually consists of two steps. In the first step, a set of discrete control gains is evaluated based on a linear control theory without considering the limits, and in the second step, appropriate gains are selected from the set of preselected discrete gains according to given criteria and rules. Yoshida *et al.*[16] have devised a control method based on this technique, to consider the limit of the control force. Fujita *et al.*[17] have proposed a control method for an AMD system to consider the limits of the auxiliary mass stroke, where four control gains are evaluated beforehand and one of these gains is selected according to several sets of inequalities expressed by the displacement and the velocity of the auxiliary mass stroke as well as several sets of rules for change of the control gains. Some other control methods based on this technique have also been proposed to consider the limits of the auxiliary mass stroke.[18,19] The problems with these VGF control techniques are: (a) it is difficult to design a proper set of discrete control gains and determine criteria for switching among the gains; (b) the control performance sometimes deteriorates due to control chattering caused by frequent discontinuous switching and (c) due to the complexity of the algorithms, it is often difficult to make clear the fundamental control characteristics. To the author's knowledge, few systematic design procedures considering the limits of the stroke length of the auxiliary mass have ever been presented for VGF control of buildings with AMD systems, yet the above-mentioned difficulties remain to be overcome for actual applications.

In this paper, a systematic design procedure and an algorithm are devised for VGF control of a building with an AMD system. The limit of the stroke length of an auxiliary mass that is regarded as principal physical constraint on AMD systems for actual applications, is considered in this design method. The proposed control method is composed of two steps. In the first step, a systematic design procedure is presented to get a set of variable feedback gains expressed as a function of a single variable that indicates a trade-off of the control performance between the reduction of the building response and the amplitude of the auxiliary mass stroke. In the second step, an efficient algorithm for controlling the variable is devised to adapt the control performance according to the variation in the intensity level of the external excitations in such a manner that the amplitude of the auxiliary mass stroke always attains a constant value within its limits. The fundamental characteristics of the proposed control method against sinusoidal base excitations are analytically investigated and key parameters that determine the control performance are defined and evaluated.

A simple design method of static output feedback controller based on LQ optimal control, is also presented. It is applicable to modal control of buildings with non-classical damping. Next, an efficient control method is developed, with combined use of the VGF control and the static output feedback control, for a hybrid structural control composed of an AMD system and passive damping devices such as oil dampers or viscous dampers. It is shown through numerical examples that the proposed control method effectively adapts the control performance according to the variation in the intensity level of the external excitations such that the amplitude of the auxiliary mass stroke is kept within its limits and the control power is restrained as well. The application range of the AMD system is thereby significantly improved compared to that achieved by the conventional constant gain feedback control.

2. VARIABLE GAIN FEEDBACK CONTROL CONSIDERING CONSTRAINTS ON AMD

2.1. Concept of variable gain feedback control

The proposed VGF control method consists of two design steps. In the first step, a set of linear quadratic (LQ) optimal gains are evaluated as a function of a single variable α that indicates a trade-off of the control performance between the reduction of the building response and the amplitude of the auxiliary mass stroke. In the second step, an efficient algorithm for on-line control of the variable α is devised to adjust the control performance with the variation in the intensity level of the external excitations while the amplitude of the auxiliary mass stroke always attains a constant value within its limits.

The state-space equations of motion for a building with n degrees of freedom (DOF) and controlled by m AMDs are

$$\dot{\mathbf{z}}(t) = \mathbf{A}\mathbf{z}(t) + \mathbf{B}\mathbf{u}(t) + \mathbf{H}\ddot{\mathbf{x}}_g(t) \tag{1}$$

where $\mathbf{z}(t)$ is the state vector $\mathbf{z}(t) = \{\dot{\mathbf{x}}(t), \mathbf{x}(t)\}^T$, $\dot{\mathbf{x}}(t)$ and $\mathbf{x}(t)$ are the velocity and displacement vectors, $\ddot{\mathbf{x}}_g(t)$ is the ground base acceleration and $\mathbf{u}(t)$ is the control force vector, respectively, and

$$\mathbf{A} = \begin{bmatrix} \mathbf{M}^{-1}\mathbf{C} & \mathbf{M}^{-1}\mathbf{K} \\ \mathbf{I} & \mathbf{0} \end{bmatrix}, \quad \mathbf{B} = \begin{bmatrix} \mathbf{M}^{-1}\mathbf{b} \\ \mathbf{0} \end{bmatrix}, \quad \mathbf{H} = \begin{bmatrix} -\mathbf{I} \\ \mathbf{0} \end{bmatrix}.$$

Matrices, $\mathbf{M}$, $\mathbf{K}$, $\mathbf{C}$, $\mathbf{I}$, $\mathbf{0}$ and $\mathbf{b}$ are the mass, the stiffness and the damping matrices, the identity matrix, the zero matrix and the location matrix which defines the locations of the control force of the AMD systems, respectively.

To gets a set of linear quadratic (LQ) optimal gains which is a function of the variable α, let the quadratic performance index be given in the following form:

$$\mathbf{J}(\alpha) = \int_0^{t_f} (\mathbf{z}^T\mathbf{Q}(\alpha)\mathbf{z} + \mathbf{u}^T\mathbf{R}(\alpha)\mathbf{u})\,dt \tag{2}$$

where t_f is the earthquake duration, $\mathbf{Q}(\alpha)$ and $\mathbf{R}(\alpha)$ are a semi-positive-definite state weighting matrix and a positive-definite control weighting matrix, respectively. The optimal control force $\mathbf{u}^*(t)$ can be obtained by minimizing $\mathbf{J}(\alpha)$ under the constraint of equation (1).

The result is given by

$$\mathbf{u}^*(t) = \mathbf{G}(\alpha)\mathbf{z}(t) \tag{3}$$

where

$$\mathbf{G}(\alpha) = -\mathbf{R}^{-1}(\alpha)\mathbf{B}^{\mathrm{T}}\mathbf{P}(\alpha)$$

$$\mathbf{P}(\alpha)\mathbf{A} + \mathbf{A}^{\mathrm{T}}\mathbf{P}(\alpha) - \mathbf{P}(\alpha)\mathbf{B}\mathbf{R}^{-1}(\alpha)\mathbf{B}^{\mathrm{T}}\mathbf{P}(\alpha) - \mathbf{Q}(\alpha) = \mathbf{0} \tag{4}$$

The unknown matrix $\mathbf{P}(\alpha)$ is found from an algebraic matrix Riccati equation (4) containing the variable α, by assuming that it is constant with respect to time.

The configuration of the quadratic performance index $\mathbf{J}(\alpha)$, i.e. weighting matrices $\mathbf{Q}(\alpha)$ and $\mathbf{R}(\alpha)$, will be defined to get the variable feedback gain matrix $\mathbf{G}(\alpha)$ in the following subsection such that the variable α indicates a trade-off of the control performance between the reduction of the building response and the amplitude of the auxiliary mass stroke. This trade-off is schematically shown in Figure 1; the amplitude of the auxiliary mass is restrained for the smaller value of α; the amplitude increases with α and this improves the control performance.

For simplicity, a linear n DOF building controlled by a single AMD system, shown in Figure 2, is considered in the following, though the control method is applicable to the cases with multiple AMD systems.

2.2. *Design of variable feedback gain*

A systematic design procedure to get the variable feedback gain matrix $\mathbf{G}(\alpha)$ that provides the trade-off illustrated in Figure 1, is presented. It contains the following procedures:

(1) Two quadratic performance indices that define two opposing control objectives are chosen and the maximum and minimum values of α are given for the indices, i.e. $\mathbf{J}(\alpha_{\max})$ is for reducing the building response and $\mathbf{J}(\alpha_{\min})$ is for restraining the amplitude of the auxiliary mass stroke.

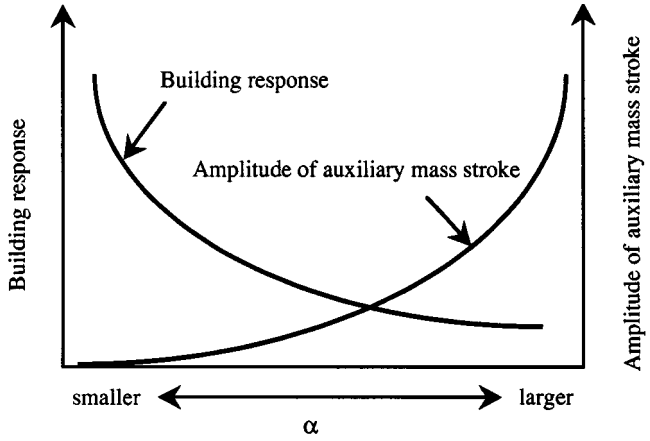

Figure 1. Trade-off of the control performance indicated by α

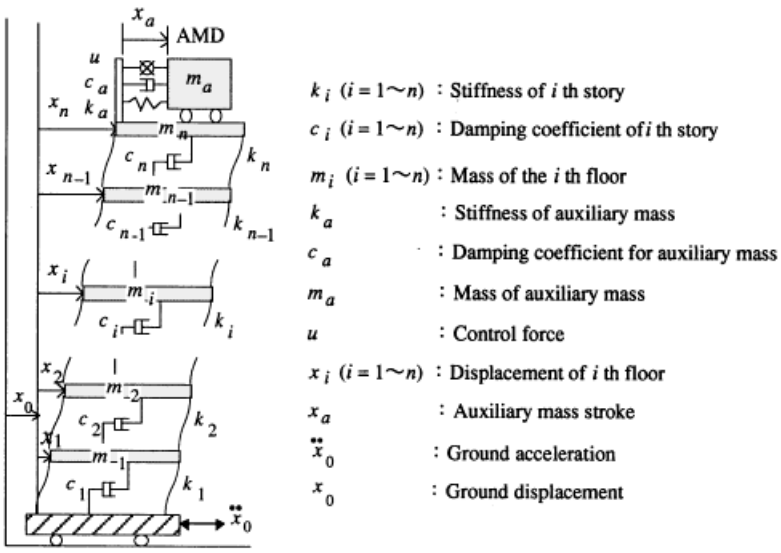

Figure 2. A prototype n DOF building–AMD model considered

(2) The configurations of weighting matrices $\mathbf{Q}(\alpha)$ and $\mathbf{R}(\alpha)$ are determined such that the performance index $\mathbf{J}(\alpha)$ would vary smoothly between the two indices by linearly changing α between $\alpha_{\min}$ and $\alpha_{\max}$.
(3) The weighting matrices $\mathbf{Q}(\alpha)$ and $\mathbf{R}(\alpha)$ are substituted into equation (4) to calculate the variable feedback gain matrix $\mathbf{G}(\alpha)$.

To realize the above-mentioned design scheme, let the state vector be arranged as

$$\mathbf{z} = [\dot{x}_1, \dot{x}_2, \ldots, \dot{x}_n, x_1, x_2, \ldots, x_n, \dot{x}_a, x_a] \tag{5}$$

where $\dot{x}_i$ and x_i are the ith floor velocity and displacement of the building and $\dot{x}_a$ and x_a are the velocity and the displacement of the auxiliary mass relative to the building floor on which the AMD is placed.

Next, the weighting matrix $\mathbf{Q}(\alpha)$ for the state vector is partitioned and given by

$$\mathbf{Q}(\alpha) = \begin{bmatrix} q_s(\alpha) \cdot \mathbf{Q}_{s2n \times 2n} & \mathbf{0}_{2n \times 2} \\ \mathbf{0}_{2 \times 2n} & q_a(\alpha) \cdot \mathbf{Q}_{a2 \times 2} \end{bmatrix} \tag{6}$$

where $q_s(\alpha)$ and $q_a(\alpha)$ are scalar functions of α, $Q_{s2n \times 2n}$ is a weighting matrix on velocities and displacements of the building floors, $\mathbf{Q}_{a2 \times 2}$ is a weighting matrix on the velocity and the displacement of the auxiliary mass relative to the building floor. $\mathbf{R}(\alpha)$, which is a scalar function in case of one AMD, is assumed to be constant.

The two opposing performance indices ($\mathbf{J}(\alpha_{\max})$ and $\mathbf{J}(\alpha_{\min})$) are given by

$$q_s(\alpha_{\max}) = q_{s\max}, \qquad q_a(\alpha_{\max}) = q_{a\min} \tag{7}$$

$$q_s(\alpha_{\min}) = q_{s\min}, \qquad q_a(\alpha_{\min}) = q_{a\max} \tag{8}$$

where ($q_{s\max}$ and $q_{a\min}$) and ($q_{s\min}$ and $q_{a\max}$) are the pairs of design parameters to be specified with $\alpha_{\max}$ and $\alpha_{\min}$; equations (7) and (8) define the control objectives for reducing the building response and restraining the amplitude of the auxiliary mass stroke, respectively.

The configuration of both $q_s(\alpha)$ and $q_a(\alpha)$ should be determined in such a manner that the performance index varies smoothly with α between the two indices. Since there is usually a difference of

exponential order between $q_{s\,max}$ and $q_{s\,min}$, or $q_{a\,min}$ and $q_{a\,max}$, these scalar functions might be given in the form

$$q_s(\alpha) = c_s \exp\left(\frac{\alpha}{d_s}\right), \qquad q_a(\alpha) = c_a \exp\left(\frac{\alpha}{d_a}\right) \tag{9}$$

where c_s, d_s, c_a, and d_a are scalar constants.

Owing to the exponential functions introduced in equation (9), the performance index as well as the resulting control performance can be varied smoothly between the two above-mentioned control objectives by linearly changing α. This will be verified and further discussed in Sections 2.5 and 4.

Substituting equations (7) and (8) into equation (9), the expressions for c_s, d_s, c_a, and d_a are obtained as

$$c_a = q_{a\,max}\left(\frac{q_{a\,max}}{q_{a\,min}}\right)^{\alpha_{min}/(\alpha_{max}-\alpha_{min})}, \qquad d_a = \frac{\alpha_{min}-\alpha_{max}}{\ln(q_{a\,max}/q_{a\,min})} \tag{10}$$

$$c_s = q_{s\,min}\left(\frac{q_{s\,min}}{q_{s\,max}}\right)^{\alpha_{min}/(\alpha_{max}-\alpha_{min})}, \qquad d_s = \frac{\alpha_{min}-\alpha_{max}}{\ln(q_{s\,min}/q_{s\,max})} \tag{11}$$

Now, since $q_s(\alpha)$ and $q_a(\alpha)$ are known, the weighting matrix $\mathbf{Q}(\alpha)$ can be determined and then substituted into equation (4) to get the variable feedback gain matrix $\mathbf{G}(\alpha)$. Since it is generally difficult to get closed-form solution of $\mathbf{G}(\alpha)$, a low-order polynomial of α is employed to fit $\mathbf{G}(\alpha)$. Samples of α, ranging between α_{min} and α_{max}, should be selected and used to fit $\mathbf{G}(\alpha)$. Eventually, the fitted polynomial for the ith element of $\mathbf{G}(\alpha)$ can be expressed as

$$\tilde{G}_i(\alpha) = g_i^0 + g_i^1 \cdot \alpha^1 + g_i^2 \cdot \alpha^2 + \cdots + g_i^L \cdot \alpha^L \tag{12}$$

where g_i^j ($j = 1$–L) are the coefficients of the Lth-order polynomial.

2.3. *Algorithm for controlling the variable* α

An efficient algorithm for on-line control of the variable α which can be installed in a computer such as a Digital Signal Processor for actual applications is devised. The variable α is changed step by step in the prescribed range of the control performance, bounded by α_{min} and α_{max}, in order to adapt the control performance to variation in the intensity level of the external excitations. In the control process, the amplitude of the auxiliary mass stroke attains a constant value within its limits.

The following parameters are introduced to describe the algorithm:

t_0	initial control time
α_{init}	initial value of α
i	denotes the ith time step
α_i	value of α at the ith time step
$\mathbf{z}_i$	state vector $\mathbf{z}$ at the ith time step
x_{ai}	amplitude of the auxiliary mass stroke at the ith time step
x_{aT}	target amplitude of the auxiliary mass stroke
x_{aL}	stroke length limit of the auxiliary mass
$\Delta\alpha$	increment of α
β_i	relative error of x_{ai} to x_{aT} at the ith time step, which is expressed as

$$\beta_i = 1{\cdot}0 - \frac{|x_{ai}|}{x_{aT}} \tag{13}$$

u_L	control force limit

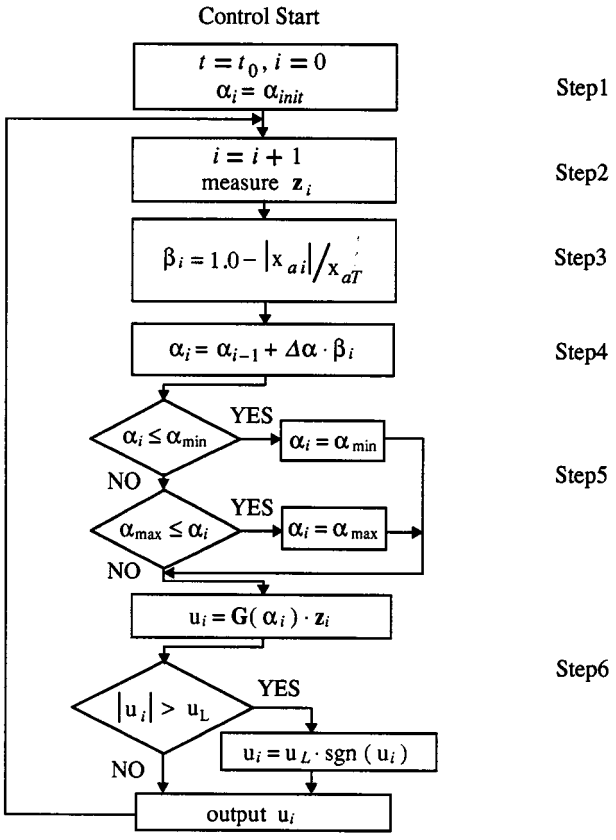

Figure 3. Flowchart of the proposed algorithm for on-line control of the variable α

The flowchart of the proposed algorithm is shown in Figure 3. It contains the following steps:

Step 1: Set $i = 0$ at the initial time t_0 and specify $\alpha_0 = \alpha_{\text{init}}$.
Step 2: Set $i = i + 1$, and measure the state vector $\mathbf{z}_i$.
Step 3: Calculate the relative error β_i.
Step 4: Change the variable α_i according to $\alpha_i = \alpha_{i-1} + \Delta\alpha \cdot \beta_i$ (14)
Step 5: Determine α_i within the range from $\alpha_{\min}$ to $\alpha_{\max}$.
Step 6: Calculate the control force $u_i = \mathbf{G}(\alpha_i) \cdot \mathbf{z}_i$ and output u_i as

$$u_i = \begin{cases} \mathbf{G}(\alpha_i) \cdot \mathbf{z}_i & \text{for} \quad |u_i| \leqslant u_L \\ u_L \operatorname{sgn}(\mathbf{G}(\alpha_i) \cdot \mathbf{z}_i) & \text{for} \quad |u_i| > u_L \end{cases}$$

The procedure is incrementally repeated from Steps 2 to 6.

It should be noted that the relative error β_i is introduced at Step 3 not only to change the variable α_i but also to avoid possible control chattering when the amplitude of auxiliary mass stroke varies in the vicinity of the target amplitude. This results in a smooth control of α_i which will be verified in Sections 2.5 and 4.

2.4. Fundamental characteristics of the proposed algorithm for controlling the variable α

Characteristics of the proposed algorithm for controlling the variable α are analytically investigated for sinusoidal base excitations, and the key parameters which determine the control performance are defined and evaluated.

Let us assume that the response of a building, in which an AMD is installed, exhibits a sinusoidal motion with circular frequency of $\omega_0 = 2\pi/T_0$, where T_0 is the corresponding period. Let the amplitude of the auxiliary mass stroke, subjected to the sinusoidal motion of the building, be denoted by P; the target amplitude by P_T; and the limit of the amplitude by P_L. The variable α is either increased or decreased step by step according to the deviation of P from the target amplitude P_T, using equation (13); α increases while $P < P_T$; decreases while $P > P_T$. An example of this oscillation of α with respect to P during the interval of T_0 is schematically shown in Figures 4(a) and 4(b). It is to be noted that this example is a particular case where α preserves the initial value of α_0 at every half-cycle of the sinusoidal motion of the building. Although P will also vary periodically with the same circular frequency, its motion may have some deviation from a pure sinusoidal motion due to the oscillation of α, as shown in Figure 4(a). It should be noted however that as long as the amplitude of oscillation of α is limited to certain range, P is assumed to exhibit a sinusoidal motion. In the following, the fundamental characteristics of the algorithm are investigated under the assumption that P exhibits a sinusoidal motion during each interval $T_0/2$.

Let Δt be the sampling time interval, given by $T_0/2N$, in which $2N$ denotes the number of the sampling time intervals during T_0. The auxiliary mass stroke at the ith time step (P_i) can be written as

$$P_i = \mu P_T \sin(\omega_0 \Delta t \cdot i) \quad (i = 0, 1, 2, \dots) \tag{15}$$

where μ denotes the ratio of the amplitude of the auxiliary mass stroke to P_T.

Applying the algorithm presented in Section 2.3, the value of α at the ith time step (α_i) is obtained for $i \leqslant N$ as follows:

$$\begin{aligned} \alpha_i &= \alpha_0 + \Delta\alpha \sum_{k=1}^{i} \beta_k = \alpha_0 + \Delta\alpha \sum_{k=1}^{i} \{1 - \mu \sin(\omega_0 \Delta t k)\} \\ &= \alpha_0 + \Delta\alpha \left\{ i - \mu \frac{\sin(\frac{1}{2} i \omega_0 \Delta t) \sin(\frac{1}{2}(i+1)\omega_0 \Delta t)}{\sin(\frac{1}{2}\omega_0 \Delta t)} \right\} \end{aligned} \tag{16}$$

where α_0 is the initial value of α.

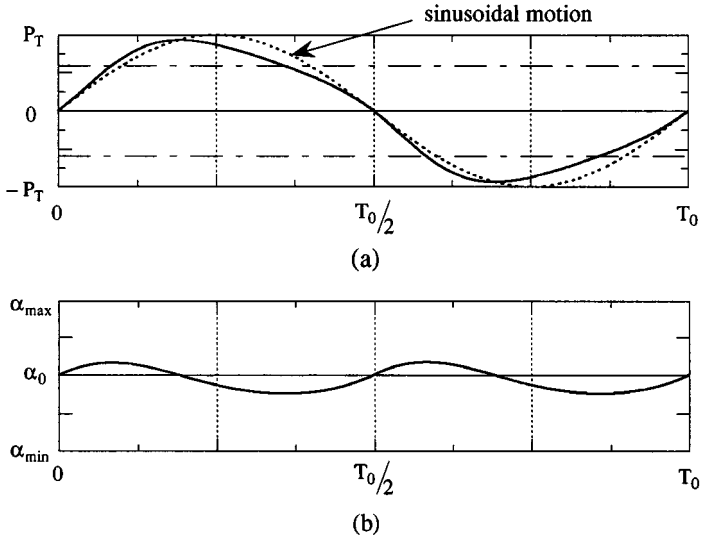

Figure 4. Schematic time-history responses for sinusoidal motion of a building: (a) amplitude of the auxiliary mass stroke; (b) oscillation of the variable α

After substituting $i = N$ into the second term of equation (16) and rearranging the equation, α_N can be written as

$$\alpha_N = \alpha_0 + \Delta\alpha\, N \left\{ 1 - \frac{\mu}{N \tan(\pi/2N)} \right\} \tag{17}$$

The second term of equation (17) expresses the difference between α_N and α_0 which is accumulated during the considered time interval $T_0/2$. If μ is equal to μ_s, which is defined by

$$\mu_s = N \tan(\pi/2N) \tag{18}$$

this difference is zero and therefore α_N remains equal to α_0 at every half-cycle of the sinusoidal motion of the auxiliary mass stroke. Two key parameters that determine the control performance of the algorithm can be defined and evaluated from equations (16)–(18).

2.4.1. Key control parameters. The first parameter is the target amplitude P_T. When μ is less than μ_S, according to the algorithm α_N is increased to amplify the amplitude of the auxiliary mass stroke, and once μ exceeds μ_S, α_N is decreased to reduce the amplitude. Thus, α_N is automatically arranged so as to keep μ close to μ_S, and hence the variable α is controlled always to keep the amplitude of the auxiliary mass stroke close to $\mu_S P_T$.

Figure 5(a) shows the relation between μ_S and N. It should be noted that

$$\lim_{N \to \infty} N \tan(\pi/2N) = \frac{\pi}{2} \tag{19}$$

It is evident from Figure 5(a) that μ_S approaches close to a value of $\pi/2$ for N more than 10. To avoid saturation of the auxiliary mass stroke when N is greater than 10, the target amplitude should be set to satisfy the following inequality:

$$P_T < P_L \Big/ \frac{\pi}{2} \tag{20}$$

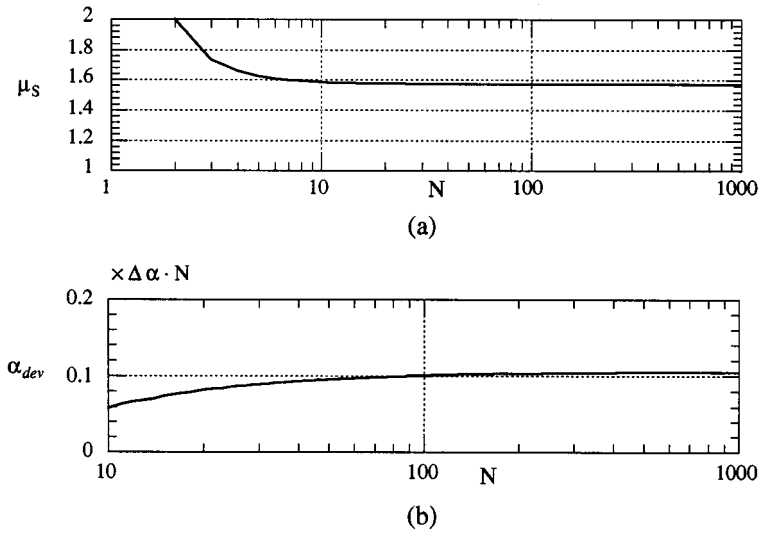

Figure 5. Variation of μ_S and amplitude of oscillation of α (α_{dev}) with respect to N: (a) μ_S vs. N; (b) α_{dev} vs. N

It should be noted again that, though the amplitude of the auxiliary mass stroke may have some deviation from a pure sinusoidal motion due to the oscillation of α, α_N will be automatically arranged so as to bring the ratio of the amplitude of the auxiliary mass stroke to the target amplitude P_T to a certain value. The above ratio is considered to be close to $\pi/2$, if the amplitude of the oscillation of α is limited to certain range.

The second parameter is response speed of the control algorithm defined by the rate of the increment of α_N to α_0 accumulated during the time interval of $T_0/2$:

$$\frac{\partial \alpha_N}{\partial \mu} = -\frac{\Delta\alpha\, N}{N \tan(\pi/2N)} \tag{21}$$

Assuming $N > 10$ and accordingly substituting $N \tan(\pi/2N) \cong \pi/2$ into equation (21) yields

$$\frac{\partial \alpha_N}{\partial \mu} \cong \frac{2}{\pi}\Delta\alpha\, N \tag{22}$$

Equation (22) shows that the response speed of the control algorithm is approximately proportional to $\Delta\alpha\, N$. According to the increase in $\Delta\alpha\, N$, the response speed as well as the amplitude of the oscillation of $\alpha(\alpha_{dev})$ will increase as well. Since excessive increase of α_{ev} may lead to deterioration in the control performance, the value of $\Delta\alpha\, N$ should be determined to keep α_{dev} within an appropriate range that enables efficient control.

Let i_S be the minimum value of i, which satisfies the following condition:

$$P_T \sin(\omega_0 \Delta t\, i) \leqslant P_T < \mu_S P_T \sin\{\omega_0 \Delta t(i+1)\} \tag{23}$$

Assuming that α_N remains the same at every half-cycle of the building response, i.e. equation (18) holds, α_{dev} can then be evaluated by substituting i_S into the second term of equation (16) as follows:

$$\alpha_{dev} = \Delta\alpha\, N \left\{ \frac{i_S}{N} - \frac{\sin(\frac{1}{2} i_S \omega_0 \Delta t) \sin(\frac{1}{2}(i_S+1)\omega_0 \Delta t)}{\cos(\frac{1}{2}\omega_0 \Delta t)} \right\} \tag{24}$$

From equation (24), the relation between $\Delta\alpha\, N$ and α_{dev} is numerically evaluated for $N > 10$ and illustrated in Figure 5(b). Apparently, α_{dev} varies from $0{\cdot}06 \times \Delta\alpha\, N \sim 0{\cdot}1 \times \Delta\alpha\, N$ and is close to $0{\cdot}1 \times \Delta\alpha\, N$ for large values of N.

In the case of application of the control algorithm to response control of a building subjected to random excitations such as wind or earthquake loads, the key parameter $\Delta\alpha\, N$ should be determined assuming a sinusoidal motion with the natural period of the building's dominant mode which is to be controlled; the first natural period of the building should be considered, since the first mode usually dominates in the response of the building top on which an AMD system is usually placed, and consequently the response of the auxiliary mass, which is usually calibrated to the first mode of the building, has the same dominant period.

2.5. Verification of the fundamental characteristics of the proposed algorithm

To verify the fundamental characteristics of the algorithm investigated in the previous subsection, numerical analyses of a SDOF building model controlled by an AMD on its top, are carried out. The stiffness, the damping coefficient and the mass of the building model are 402·84 tonf*/m, 2·56 tonf sec/m and 100 ton, respectively, and the first natural period is 1 sec. Parameters of the auxiliary mass are calibrated to the natural frequency of the building using the Den Hartog formula developed for conventional tuned mass damper (TMD);[20] the mass is 1 ton or 1 per cent of the building mass, and the stiffness and the damping coefficients are 3·95 tonf/m and $7{\cdot}66 \times 10^{-2}$ tonf sec/m, respectively.

* 1 tonf = 9·807 kN

2.5.1. Design of variable feedback gain. A state vector for the building–AMD system is arranged as

$$\mathbf{z} = [\dot{x}_1, x_1, \dot{x}_a, x_a]$$

and the weighting matrix $\mathbf{Q}(\alpha)$, which is partitioned in the same way as equation (6), is given by

$$\mathbf{Q}(\alpha) = \begin{bmatrix} q_s(\alpha) \cdot \mathbf{Q}_{s2\times 2} & \mathbf{0}_{2\times 2} \\ \mathbf{0}_{2\times 2} & q_a(\alpha) \cdot \mathbf{Q}_{a2\times 2} \end{bmatrix}$$

where $\mathbf{Q}_{s2\times 2}$ and $\mathbf{Q}_{a2\times 2}$ are chosen as follows:

$$\mathbf{Q}_{s2\times 2} = \begin{bmatrix} 1{\cdot}0 & \\ & 1{\cdot}0 \end{bmatrix}, \qquad \mathbf{Q}_{a2\times 2} = \begin{bmatrix} 0{\cdot}0 & \\ & 1{\cdot}0 \end{bmatrix}$$

$\mathbf{R}(\alpha)$ is fixed at $1{\cdot}0\times 10^{-2}$. $q_{s\,max} = 1{\cdot}0$ and $q_{a\,min} = 1{\cdot}0\times 10^{-2}$ are chosen with $\alpha_{max} = 2{\cdot}0$ to define the performance index for the reduction of the building response and $q_{s\,min} = 1{\cdot}0\times 10^{-2}$ and $q_{a\,max} = 10{\cdot}0$ are chosen with $\alpha_{min} = 0{\cdot}2$ to define the performance index for restraining the amplitude of the auxiliary mass stroke.

A fourth-order polynomial of α is employed to fit the curves of the variable feedback gain matrix $\mathbf{G}(\alpha)$, by using the least-squares technique. Samples of α, ranging between 0·2 and 2·0, i.e. 0·2, 0·4, 0·6, 0·8, 1·0, 1·2, 1·4, 1·6, 1·8, and 2·0, are selected to calculate $\mathbf{G}(\alpha)$ and each element of $\mathbf{G}(\alpha)$ is normalized by the corresponding element of a constant feedback gain matrix $\mathbf{G_0}$ that is calculated for $\alpha_{min} = 0{\cdot}2$. Figure 6 shows the normalized feedback gains, where circular and triangular marks indicate the samples of the variable feedback gains calculated for the samples of α and the solid lines indicate the fitted polynomial curves. To assess the overall fit of the curve to the data, the following statistic R_i^2 (Reference 21) for the ith element of $\mathbf{G}(\alpha)$ is evaluated:

$$R_i^2 = \frac{\sum_{k=1}^{n} (\tilde{G}_i(\alpha_k) - \bar{G}_i)^2}{\sum_{k=1}^{n} (G_i(\alpha_k) - \bar{G}_i)^2} \times 100\% \tag{25}$$

where n is number of the samples of α, α_k denotes the kth sample of α, $G_i(\alpha_k)$ is the sample of the ith element of $\mathbf{G}(\alpha)$ calculated for α_k, $\tilde{G}_i(\alpha_k)$ is the sample of the fitted ith element of $\mathbf{G}(\alpha)$ for α_k and $\bar{G}_i$ is the mean of $G_i(\alpha_k)$. R_i^2 for each element of $\mathbf{G}(\alpha)$ were all greater than 99·9 per cent and close to the perfect fitting, which is associated with a value of $R_i^2 = 100$ per cent.

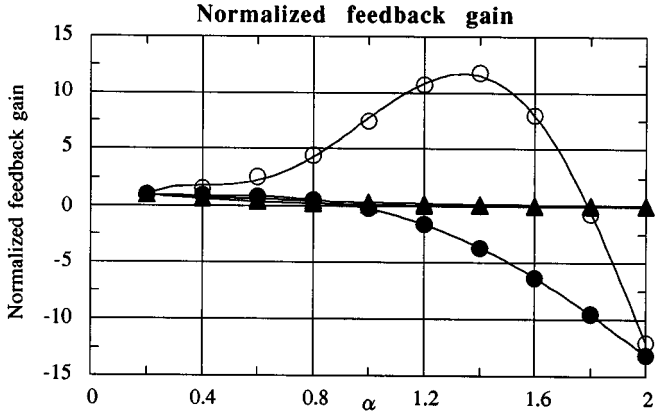

Figure 6. Normalized feedback gain for a SDOF building–AMD system: (—●—) feedback gain for displacement of the building; (—▲—) feedback gain for relative displacement of the auxiliary mass to the building; (—○—) feedback gain for velocity of the building; (—△—) feedback gain for relative velocity of the auxiliary mass with respect to the building

The frequency response functions (FRF) of the SDOF building–AMD system under base excitations are evaluated for different values of α. The FRF for the displacement response of the building which is normalized by the maximum amplitude of the FRF for the case without control, is shown in Figure 7(a). The FRF for the amplitude of the auxiliary mass stroke which is normalized by the maximum amplitude of the FRF for a passive TMD, is shown in Figure 7(b). It is apparent that the maximum amplitudes of the FRF for the displacement response of the building and for the amplitude of the auxiliary mass stroke have opposite tendencies with the change of the variable α. This demonstrates the trade-off of the control performance illustrated in Figure 1.

2.5.2. Response analysis. To evaluate and verify the fundamental characteristics of the proposed VGF control over a wide range of excitation intensities, a modified sinusoidal ground acceleration with a circular frequency of 2π rad/sec, is scaled to different peak ground acceleration (PGA) and used as the input base excitation. The time history of the ground acceleration is shown in Figure 8; duration of the excitation is

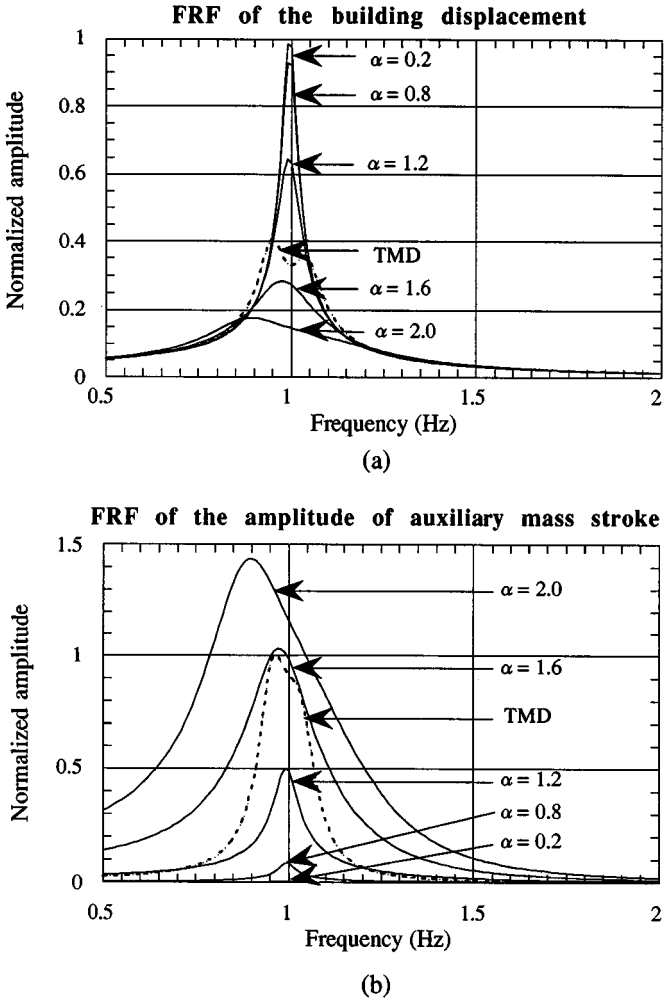

Figure 7. FRF of the SDOF building–AMD system under base excitations: (a) FRF of the building displacement; (b) FRF of the amplitude of auxiliary mass stroke

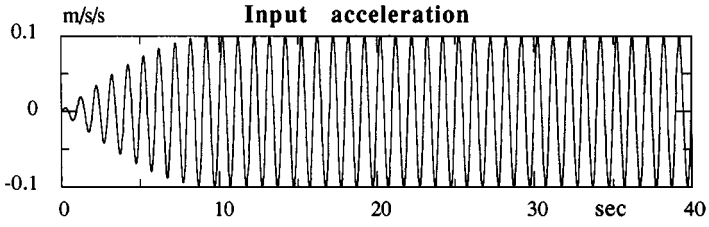

Figure 8. Time history of the modified sinusoidal ground acceleration

40 sec and the first 5 sec are enveloped by a sinusoidal curve with a circular frequency of 0·4 π rad/sec. The sampling time interval Δt is 0·02 sec and hence the number of the time intervals per half-cycle of the excitation is $N = 25$. The two key parameters, defined and discussed in Section 2·4, are chosen as follows: the target amplitude of the auxiliary mass stroke is $x_{aT} = 0{\cdot}15$ m and the increment of α is $\Delta\alpha = 0{\cdot}015$, which corresponds to $\Delta\alpha\, N = 0{\cdot}375$ and in fact, determines the response speed of the control. The control force limit u_L is taken to be 1 tonf.

The response reduction ratio, which is defined by the ratio of the maximum response amplitude of the building displacement to the corresponding response for the case without control, is plotted for different intensities of the excitations in Figure 9(a). Similarly, the maximum response amplitude of the auxiliary mass stroke, which is normalized by the target amplitude x_{aT}, is plotted in Figure 9(b). In these figures, the thin solid lines indicate results for different values of α and the thin dotted line indicates the case with a passive TMD. In Figure 9(b), steady-state amplitudes of the auxiliary mass stroke, which are observed toward the end of the sinusoidal excitations, are also plotted and indicated by the thick solid line. As illustrated in Figure 9(b), the steady-state amplitude of the auxiliary mass stroke attains a value of $\pi/2 \times x_{aT}$, and at the same time the maximum amplitude of the auxiliary mass stroke is restricted to approximately $2{\cdot}2 \times x_{aT}$.

To compare the control performance of the VGF control with that of constant gain feedback (CGF) controls, the CGF controls which have the same response reduction ratio as the VGF control are indicated by cross marks in Figure 9(a), for the different intensities of the input excitation. In the same manner, the maximum amplitudes of the auxiliary mass stroke with corresponding CGF controls are indicated in Figure 9(b). It should be noted that the cross marks in Figure 9(b) lie along the thick solid line. This indicates that the performance of the VGF control is automatically adapted for different intensity levels of the input excitations and attains that of the CGF control with the maximum amplitude of the auxiliary mass stroke equal to $\pi/2 \times x_{aT}$. The difference between the maximum and the steady-state amplitude of the auxiliary mass stroke denotes the margin which should be considered in determining the target response amplitude that satisfies the inequality condition (20).

The time-history responses of the SDOF building–AMD system, subjected to a sinusoidal base excitation with PGA of 0·4 m/sec/sec, are shown in Figure 10; the displacement of the building, the amplitude of the auxiliary mass stroke, the control force and the variable α are shown in the figure. It is apparent that the variable α is controlled such that the amplitude of the auxiliary mass stroke attains a value of $\pi/2 \times x_{aT}$. The amplitude of the oscillation of α toward the end of the excitation is approximately 0·04 and close to $0{\cdot}1 \times \Delta\alpha\, N$, as discussed in Section 2.4. Though the influence of this oscillation of α is observed in the control force, the amplitude of the auxiliary mass stroke still resembles a sinusoidal motion.

3. DESIGN OF STATIC OUTPUT FEEDBACK CONTROLLER

Static output feedback (SOF) control is necessary for the proposed VGF control in actual applications, since it is not practical to measure the full state vector of a building–AMD system. One solution to this problem is

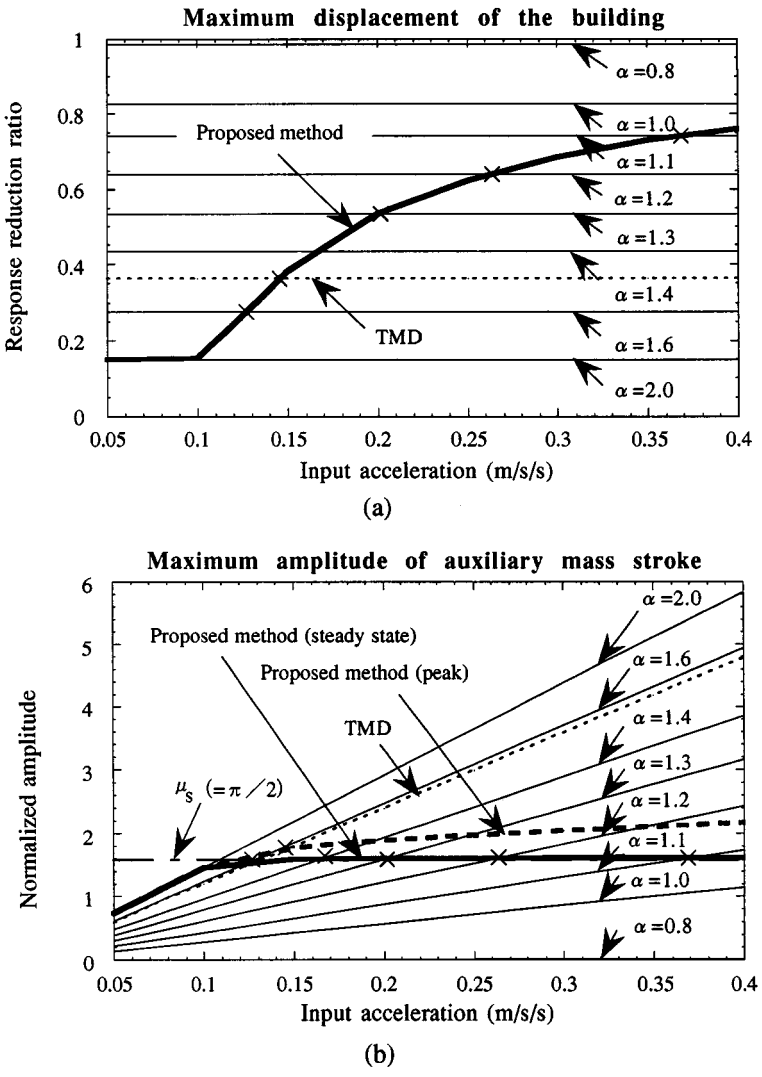

Figure 9. Maximum responses of the SDOF building–AMD system subjected to sinusoidal base excitations: (a) response reduction ratio for the maximum displacement of the building; (b) maximum amplitude of auxiliary mass stroke

to apply an optimal output feedback control, for which several algorithms to compute the optimal gains have been already investigated and developed.[22–24] In this section, however, a simple design method of SOF controller based on LQ optimal control is reviewed.[25,26] The practical significance of this method is its applicability to modal control of a building with non-classical damping and accordingly to hybrid structural control combined with AMD systems and passive damping devices such as oil dampers or viscous dampers. A reduced order model as well as a reduced weighting matrix for optimal control of the considered modes are obtained through canonical transformation of the state-space equation of the system. The evaluation of the output feedback gains by considering complex modes is described in the following.

Let us consider the following complex eigenproblem:

$$\mathbf{\Phi\Lambda} = \mathbf{A\Phi} \tag{26}$$

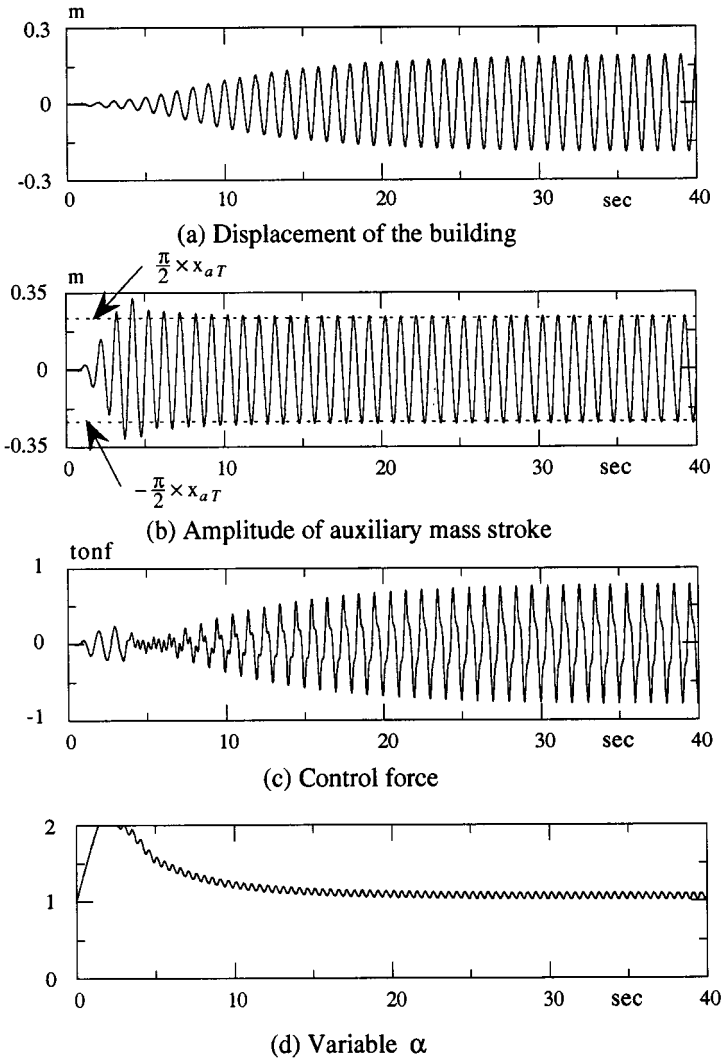

Figure 10. Time-history responses of the SDOF building–AMD system subjected to sinusoidal base excitation with 0·4 m/sec/sec PGA

where

$$\mathbf{\Lambda} = \begin{bmatrix} \mathbf{R}_1 & & \\ & \mathbf{R}_i & \\ & & \mathbf{R}_N \end{bmatrix} \tag{27}$$

and $\mathbf{R}_i$ is a diagonal 2×2 matrix, containing a conjugate pair of complex eigenvalues. Let

$$\lambda_i = \xi_i + \mathrm{j}\eta_i, \quad \bar{\lambda}_i = \xi_i - \mathrm{j}\eta_i$$

be a pair of conjugate complex eigenvalues, where ξ_i and η_i are both real, $\eta_i > 0$ and $\mathrm{j} = \sqrt{-1}$. The eigenvector $\boldsymbol{\phi}^i$ that corresponds to λ_i is also complex. Let $\boldsymbol{\sigma}^i$ and $\boldsymbol{\tau}^i$ be real vectors determined by

$$\boldsymbol{\phi}^i = \boldsymbol{\sigma}^i + \mathrm{j}\boldsymbol{\tau}^i \tag{28}$$

By replacing the two conjugate complex eigenvectors of $\mathbf{\Phi}$ that correspond to λ_i and $\bar{\lambda}_i$ by $\boldsymbol{\sigma}^i$ and $\boldsymbol{\tau}^i$, respectively, the following real matrix $\mathbf{T}$ is obtained:

$$\mathbf{T} = [\boldsymbol{\sigma}^1, \boldsymbol{\tau}^1, \dots, \boldsymbol{\sigma}^i, \boldsymbol{\tau}^i, \dots] \tag{29}$$

Next, a co-ordinate transformation:

$$\mathbf{z}(t) = \mathbf{\Phi}\,\mathbf{q}(t) \tag{30}$$

where $\mathbf{q}(t)$ is the real modal vector of generalized co-ordinates, is introduced.[27]

By using this transformation, the state-space equation (1) as well as the quadratic performance index given by equation (2) can be transformed into generalized co-ordinates as follows:

$$\dot{\mathbf{q}}(t) = \tilde{\mathbf{\Lambda}}\,\mathbf{q}(t) + \mathbf{\Gamma}\,\mathbf{u}(t) + \Xi\ddot{\mathbf{x}}_{\mathrm{g}}(t) \tag{31}$$

$$\mathbf{J}(\alpha) = \int_0^{t_{\mathrm{f}}} (\mathbf{q}^{\mathrm{T}}\tilde{\mathbf{Q}}(\alpha)\mathbf{q} + \mathbf{u}^{\mathrm{T}}\mathbf{R}(\alpha)\mathbf{u})\,\mathrm{d}t \tag{32}$$

where $\tilde{\mathbf{\Lambda}} = \mathbf{T}^{-1}\mathbf{A}\mathbf{T}$, $\mathbf{\Gamma} = \mathbf{T}^{-1}\mathbf{B}$, $\Xi = \mathbf{T}^{-1}\mathbf{H}$, $\tilde{\mathbf{Q}}(\alpha) = \mathbf{T}^{-1}\mathbf{Q}(\alpha)\mathbf{T}$ and $\tilde{\mathbf{\Lambda}}$ has the following form:

$$\tilde{\mathbf{\Lambda}} = \begin{bmatrix} \tilde{\mathbf{R}}_1 & & \\ & \tilde{\mathbf{R}}_i & \\ & & \tilde{\mathbf{R}}_N \end{bmatrix} \tag{33}$$

in which

$$\tilde{\mathbf{R}}_i = \begin{bmatrix} \xi_i & \eta_i \\ -\eta_i & \xi_i \end{bmatrix} \tag{34}$$

Equation (31) expresses $n+1$ sets of two coupled first-order differential equations with real coefficients. Each set of the differential equations is mutually uncoupled and has real coefficients and, consequently, LQ optimal control can be combined with the modal control as shown in the following.

Assuming that only a certain ordered number of lower modes are to be controlled, the modal vector can be partitioned into controlled modes ($\mathbf{q}_{\mathrm{C}}(t)$) and residual modes ($\mathbf{q}_{\mathrm{R}}(t)$). Other vectors and matrices can be partitioned in a similar way as follows:

$$\mathbf{q}(t) = \begin{bmatrix} \mathbf{q}_{\mathrm{C}}(t) \\ \mathbf{q}_{\mathrm{R}}(t) \end{bmatrix}, \quad \tilde{\mathbf{\Lambda}} = \begin{bmatrix} \tilde{\mathbf{\Lambda}}_{\mathrm{C}} & \mathbf{0} \\ \mathbf{0} & \tilde{\mathbf{\Lambda}}_{\mathrm{R}} \end{bmatrix}, \quad \mathbf{\Gamma} = \begin{bmatrix} \mathbf{\Gamma}_{\mathrm{C}} \\ \mathbf{\Gamma}_{\mathrm{R}} \end{bmatrix}, \quad \Xi = \begin{bmatrix} \Xi_{\mathrm{C}} \\ \Xi_{\mathrm{R}} \end{bmatrix} \tag{35}$$

$$\tilde{\mathbf{Q}}(\alpha) = \begin{bmatrix} \tilde{\mathbf{Q}}_{\mathrm{CC}}(\alpha) & \tilde{\mathbf{Q}}_{\mathrm{CR}}(\alpha) \\ \tilde{\mathbf{Q}}_{\mathrm{RC}}(\alpha) & \tilde{\mathbf{Q}}_{\mathrm{RR}}(\alpha) \end{bmatrix} \tag{36}$$

Equations of the controlled and the residual modes can be written in the following form:

$$\dot{\mathbf{q}}_{\mathrm{C}}(t) = \tilde{\mathbf{\Lambda}}_{\mathrm{C}}\mathbf{q}_{\mathrm{C}}(t) + \mathbf{\Gamma}_{\mathrm{C}}\,\mathbf{u}(t) + \Xi_{\mathrm{C}}\ddot{\mathbf{x}}_{\mathrm{g}}(t) \tag{37a}$$

$$\dot{\mathbf{q}}_{\mathrm{R}}(t) = \tilde{\mathbf{\Lambda}}_{\mathrm{R}}\mathbf{q}_{\mathrm{R}}(t) + \mathbf{\Gamma}_{\mathrm{R}}\,\mathbf{u}(t) + \Xi_{\mathrm{R}}\ddot{\mathbf{x}}_{\mathrm{g}}(t) \tag{37b}$$

To eliminate the effects of the weighting matrix on the residual modes, $\tilde{\mathbf{Q}}_{\mathrm{CR}}(\alpha) = \tilde{\mathbf{Q}}_{\mathrm{RC}}(\alpha) = \tilde{\mathbf{Q}}_{\mathrm{RR}}(\alpha) = \mathbf{0}$ is assumed in equation (36), and the quadratic performance index for the controlled modes $\mathbf{J}_{\mathrm{C}}(\alpha)$ is expressed as

$$\mathbf{J}_{\mathrm{C}}(\alpha) = \int_0^{t_{\mathrm{f}}} (\mathbf{q}_{\mathrm{C}}^{\mathrm{T}}\tilde{\mathbf{Q}}_{\mathrm{CC}}(\alpha)\mathbf{q}_{\mathrm{C}} + \mathbf{u}^{\mathrm{T}}\mathbf{R}(\alpha)\mathbf{u})\,\mathrm{d}t \tag{38}$$

The optimal control force for the controlled modes, $\mathbf{u}_C^*(t)$, can be obtained by minimizing $\mathbf{J}_C(\alpha)$ under the constraint of equation (37a). The result is given by

$$\mathbf{u}_C^*(t) = \mathbf{G}_C(\alpha)\mathbf{q}_C(t) \tag{39}$$

in which

$$\mathbf{G}_C(\alpha) = -\mathbf{R}^{-1}(\alpha)\boldsymbol{\Gamma}_C^T\mathbf{P}_C(\alpha) \tag{40}$$

$$\mathbf{P}_C(\alpha)\tilde{\boldsymbol{\Lambda}}_C + \tilde{\boldsymbol{\Lambda}}_C^T\mathbf{P}_C(\alpha) - \mathbf{P}_C(\alpha)\boldsymbol{\Gamma}_C\mathbf{R}^{-1}(\alpha)\boldsymbol{\Gamma}_C^T\mathbf{P}_C(\alpha) - \tilde{\mathbf{Q}}_{CC}(\alpha) = \mathbf{0} \tag{41}$$

The unknown matrix $\mathbf{P}_C(\alpha)$ is found from an algebraic matrix Riccati equation (41) that includes α by assuming that it is constant with respect to time.

A vector $\mathbf{Y}(t)$ of the measured displacements and velocities is the output vector

$$\mathbf{Y}(t) = \mathbf{C}\mathbf{z}(t) = \mathbf{C}_C\mathbf{q}_C(t) + \mathbf{C}_R\mathbf{q}_R(t) \tag{42}$$

where $\mathbf{C}$ is the observation matrix and $\mathbf{C}_C$ and $\mathbf{C}_R$ are obtained by an appropriate partitioning of $\mathbf{CT}$:

$$\mathbf{CT} = [\mathbf{C}_C \;\; \mathbf{C}_R] \tag{43}$$

The control algorithm described above requires the modal displacements and the modal velocities of the controlled modes. By neglecting the contribution of the residual modes in equation (42), these modal states can be estimated from the output vector $\mathbf{Y}(t)$, if inverse of the matrix $\mathbf{C}_C$ exists, as follows:

$$\mathbf{q}_C(t) \cong \mathbf{C}_C^{-1}\mathbf{Y}(t) \tag{44}$$

Substituting equation (44) into equation (39), the approximate optimal control force for the controlled modes is obtained as

$$\mathbf{u}_C^*(t) = \mathbf{G}_C(\alpha)\mathbf{C}_C^{-1}\mathbf{Y}(t) \tag{45}$$

and, finally, the state-space equation of the controlled building is given by

$$\dot{\mathbf{z}}(t) = (\mathbf{A} + \mathbf{B}\mathbf{G}_C(\alpha)\mathbf{C}_C^{-1}\mathbf{C})\mathbf{z}(t) + \mathbf{H}\ddot{x}_g(t) \tag{46}$$

By neglecting the contribution of the residual modes in equation (44), an observation spillover[28] might be caused and this may lead to performance deterioration or even instability in some cases, particularly for the lightly damped residual models. When unacceptable performance deterioration or instability occurs, compensation can be added to reduce the effects of the observation spillover. One form of this compensation is a sensor prefilter; the sensor outputs pass through this prefilter and the observation spillover is electronically removed. Another approach is the use of spatial modal filters,[29] which however may require an increase in the number of sensors to guarantee the accuracy of the modal filters. It should be noted that as long as the observation spillover is eliminated or reduced to an acceptable level, the control spillover usually causes little deterioration in the control performance.

Through comparative analyses,[25] it was demonstrated that, as long as the controlled modes are restricted to the lower modes of a building–AMD system, e.g. up to the fourth mode, and in addition to that, the velocities and the displacements of the AMD and of the floor on which the AMD is placed are included in the observation vector, the control performance usually suffers little deterioration due to the observation spillover even without compensation. Based on these findings, no compensation is made for the observation spillover, in the application example presented in Section 4; controlled modes are restricted up to the third mode of a building–AMD system, and the velocities and the displacements of an AMD as well as of the floor on which the AMD is placed are included in the observation vector.

4. APPLICATION TO HYBRID STRUCTURAL CONTROL

In order to provide high damping factors, e.g. up to 10 per cent, for the lower modes of tall buildings by means of passive dampers such as oil dampers or viscous dampers, extremely high damping coefficients are required for the dampers.[30] It is therefore considered as appropriate and effective to use passive dampers with relatively low damping coefficients that provide high damping factors for the higher modes, and to use an AMD system that provides high damping factors for a limited number of lower modes. The proposed VGF control is combined with the SOF control presented in Section 3 and then applied to a hybrid structural control, which is composed of an AMD system and passive dampers, to improve the habitability of tall buildings subjected to wind and earthquake excitations.

To demonstrate the effectiveness of the proposed VGF control combined with the SOF control, numerical analyses are carried out for a 10 DOF building model controlled both by an AMD on its top and by passive dampers installed at all stories. The stiffnesses of the first to the 10th storey are: 15 400, 14 400, 13 700, 12 900, 12 100, 11 200, 9930, 8310, 6180 and 3540 tonf/m, respectively. An equal mass of 100 ton is assumed for each floor. The corresponding natural periods are: 1·20, 0·47, 0·30, 0·22, 0·17, 0·14, 0·12, 0·11, 0·098 and 0·089 sec. The damping coefficient provided by the passive dampers is chosen as 50·0 tonf sec/m for each storey. The modal damping factors provided by the passive dampers as well as the inherent structural modal damping factors assumed as 1 per cent for all modes, are evaluated by complex eigenvalue analysis as: 2·14, 5·73, 9·37, 11·8, 13·0, 13·4, 13·7, 13·9, 14·1 and 13·9 per cent. The configuration of these modal damping factors indicates that high damping factors for the higher modes are relatively easily provided by the passive dampers. An AMD system is then added to provide high damping factors for a limited number of lower modes, in particular for the first mode. Parameters of the auxiliary mass are calibrated to the first natural frequency using the Den Hartog formula developed for TMD;[20] the mass is 4·14 ton, i.e. 1 per cent of the generalized first modal mass of the building and the stiffness and the damping coefficients are 11·29 tonf/m and $2{\cdot}64 \times 10^{-1}$ tonf sec/m, respectively.

4.1. Design of variable feedback gain

A state vector for the building–AMD system is arranged in the same way as equation (5), and the corresponding weighting matrix is given by

$$\mathbf{Q}(\alpha) = \begin{bmatrix} q_{\mathrm{s}}(\alpha) \cdot \mathbf{Q}_{\mathrm{s}10\times10} & \mathbf{0}_{2\times2} \\ \mathbf{0}_{2\times2} & q_{\mathrm{a}}(\alpha) \cdot \mathbf{Q}_{\mathrm{a}2\times2} \end{bmatrix}$$

in which $\mathbf{Q}_{\mathrm{s}10\times10}$ is chosen as an identity matrix and $\mathbf{Q}_{\mathrm{a}2\times2}$ is given as

$$\mathbf{Q}_{\mathrm{a}2\times2} = \begin{bmatrix} 0{\cdot}0 & \\ & 1{\cdot}0 \end{bmatrix}$$

$\mathbf{R}(\alpha)$ is fixed at $5{\cdot}0 \times 10^{-3}$. $q_{\mathrm{s\,max}} = 1{\cdot}0$ and $q_{\mathrm{a\,min}} = 1{\cdot}0 \times 10^{-2}$ are chosen with $\alpha_{\max} = 2{\cdot}0$ to define the performance index for the reduction of the building response; and $q_{\mathrm{s\,min}} = 1{\cdot}0 \times 10^{-2}$ and $q_{\mathrm{a\,max}} = 10{\cdot}0$ are chosen with $\alpha_{\min} = 0{\cdot}2$ to define the performance index for restraining the amplitude of the auxiliary mass stroke.

The observation vector is chosen as

$$\mathbf{z} = [\dot{x}_5, \dot{x}_{10}, x_5, x_{10}, \dot{x}_{\mathrm{a}}, x_{\mathrm{a}}]$$

where displacements and velocities of both the fifth and the top floor as well as the displacement and the velocity of the auxiliary mass relative to the top floor, on which the AMD is placed, are utilized. The first three modes of the building–AMD system are chosen for the controlled modes and the output feedback gain matrix for the observation vector is evaluated by the design method presented in Section 3.

A fourth-order polynomial of α is employed to fit the curves of the variable feedback gain matrix $\mathbf{G}(\alpha)$, using the least-squares technique. Samples of α, ranging between 0·2 and 2·0, i.e. 0·2, 0·4, 0·6, 0·8, 1·0, 1·2, 1·4,

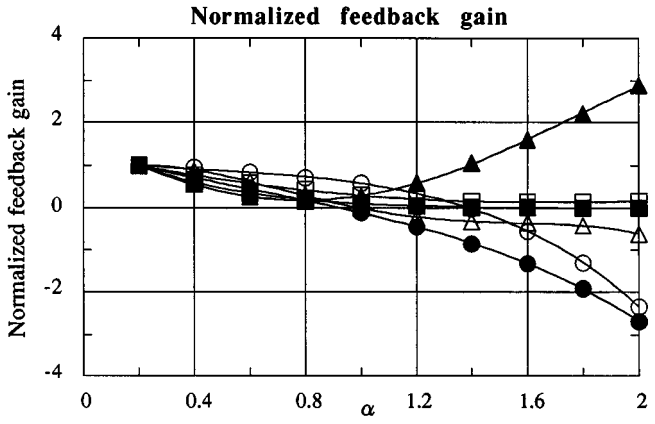

Figure 11. Normalized feedback gain for a 10 DOF building–AMD system: (—●—) feedback gain for displacement of the top floor; (—▲—) feedback gain for displacement of the fifth floor; (—■—) feedback gain for relative displacement of the auxiliary mass to the top floor; (—○—) feedback gain for velocity of the top floor; (—△—) feedback gain for velocity of the fifth floor; (—□—) feedback gain for relative velocity of the auxiliary mass to the building

1·6, 1·8 and 2·0, are selected to calculate $\mathbf{G}(\alpha)$ and each element of $\mathbf{G}(\alpha)$ is normalized by the corresponding element of the constant feedback gain matrix $\mathbf{G_0}$. Figure 11 shows the normalized feedback gains, where the symbols indicate the samples of the variable feedback gains calculated for the samples of α, and the solid lines indicate the fitted polynomial curves. The statistic R_i^2's for all elements of $\mathbf{G}(\alpha)$ were found to be all greater than 99·9 per cent and thus close to the perfect fitting.

The FRF of the building–AMD system under base excitations are evaluated for different values of α. The FRF for the top floor displacement of the building, which is normalized by the maximum amplitude of that obtained for the case without control, is shown in Figure 12(a). Similarly, the FRF for the amplitude of the auxiliary mass stroke, which is normalized by the maximum amplitude of that obtained by a passive TMD and the passive dampers, is shown in Figure 12(b). Apparently, the maximum amplitudes of the FRF for the top floor displacement and for the amplitude of the auxiliary mass stroke have opposite tendencies with the change of the variable α. This tendency is identical to that observed in the one DOF building–AMD system.

4.2. Response analysis

To verify the effectiveness of the proposed VGF control over a wide range of excitation intensities, the N–S component of the 18 May 1940 El-Centro Earthquake, shown in Figure 13, is scaled to different PGA and used as input base excitations. The limit of the auxiliary mass stroke, x_{aL}, and the control force, u_L, are given as 0.50 m and 2 tonf, respectively. The sampling time interval Δt is 0·02 sec and hence the number of time intervals per half-cycle of the first natural period of the building, N, equals 30. The two key parameters are specified as follows: $x_{aT} = 0{\cdot}15$ m and $\Delta\alpha = 0{\cdot}015$, leading to $\Delta\alpha N = 0{\cdot}45$.

The response reduction ratio of the top floor, as previously defined, is plotted for different intensities of the excitation in Figure 14(a). Equivalent plots for the maximum amplitude of the auxiliary mass stroke, normalized by x_{aT}, is shown in Figure 14(b). Though the maximum amplitude of the auxiliary mass stroke reaches approximately $3{\cdot}0 \times x_{aT}$ at PGA of 1·0 m/sec/sec, its increase is restrained for PGA above 1·0 m/sec/sec as shown in Figure 14(b). Compared to the maximum amplitude of $2.2 \times x_{aT}$ observed for sinusoidal base excitations in Section 2.5, rather large margin is required between the target amplitude and the stroke limit to avoid saturation of the auxiliary mass stroke for the case of earthquake excitations.

To compare the control performance of the VGF control with that of CGF controls, the CGF controls which have the same response reduction ratio as the VGF control and the corresponding maximum

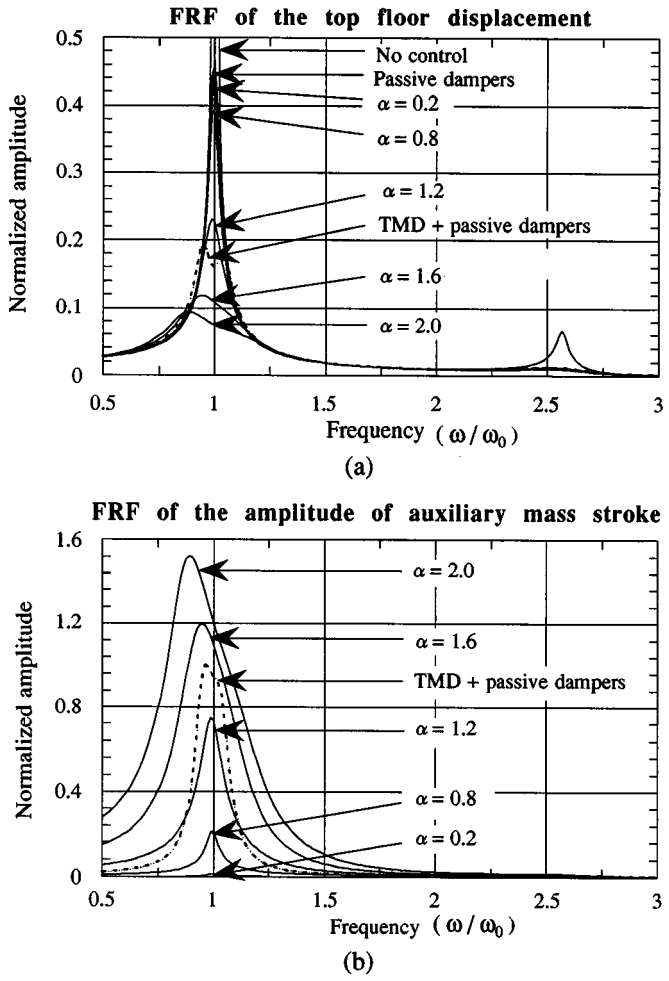

Figure 12. FRF of the 10 DOF building–AMD system under base excitations: (a) FRF of the top floor displacement; (b) FRF of the amplitude of auxiliary mass stroke

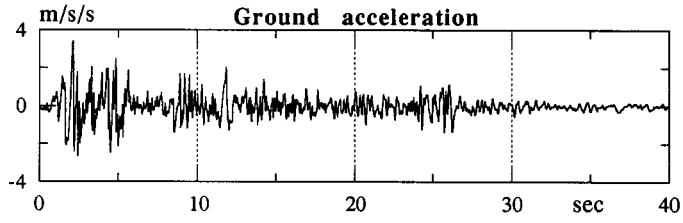

Figure 13. Time history of the N–S component of the 18 May 1940 El-Centro Earthquake

amplitudes of the auxiliary mass stroke are indicated by cross marks in Figures 14(a) and 14(b), respectively. It can be seen in Figure 14(b) that in order to achieve the same response reduction ratio, the proposed VGF control requires slightly larger maximum amplitude of the auxiliary mass stroke than that of the CGF controls. However, it is shown that the proposed VGF control effectively adapts the control performance to

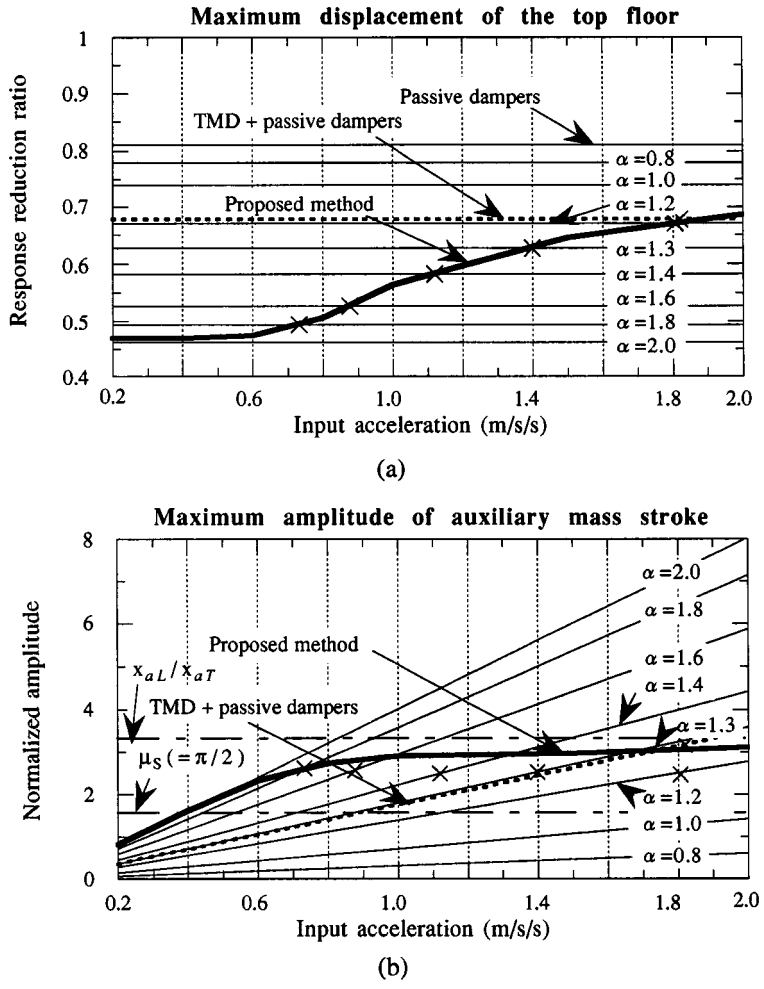

Figure 14. Maximum responses of the 10 DOF building–AMD system subjected to 1940 El-Centro NS Earthquake excitations: (a) response reduction ratio for the maximum displacement of the top floor; (b) maximum amplitude of auxiliary mass stroke

variation in the intensity level of both seismic and sinusoidal excitations in such a manner that the amplitude of the auxiliary mass stroke is kept within its limits.

The maximum control power and the maximum control force which are required for both the VGF control and the CGF control are summarized in Table I. The variable α is fixed at 2·0 and the maximum control force is limited to 2·0 tonf for the CGF control. As listed in Table I, the maximum control power increases considerably for the CGF control with the increase in PGA of the input excitation even if the control force is limited. On the contrary, the increase of the maximum control power is restrained for the VGF control.

The time-history responses of the building–AMD system, subjected to El-Centro NS ground motion with PGA of 2·0 m/sec/sec, are shown in Figure 15. Apparently, the variable α is smoothly controlled, and therefore, no control chattering is observed in the control force. The variable α immediately increases up to 2·0 toward the end of the excitation to suppress the free vibration of the building following the seismic excitation.

Table I. Maximum control force and maximum control power for VGF control and CGF control with $\alpha = 2{\cdot}0$

Input acceleration (m/sec/sec)	Maximum control force (tonf)		Maximum control power (kw)	
	CGF control	VGF control	CGF control	VGF control
0·2	0·55	0·54	2·38	2·45
0·4	1·08	1·08	9·50	9·79
0·6	1·57	1·62	21·4	18·3
0·8	2·00	2·00	38·1	22·2
1·0	2·00	2·00	53·3	29·1
1·5	2·00	2·00	85·6	35·9
2·0	2·00	2·00	103	41·1

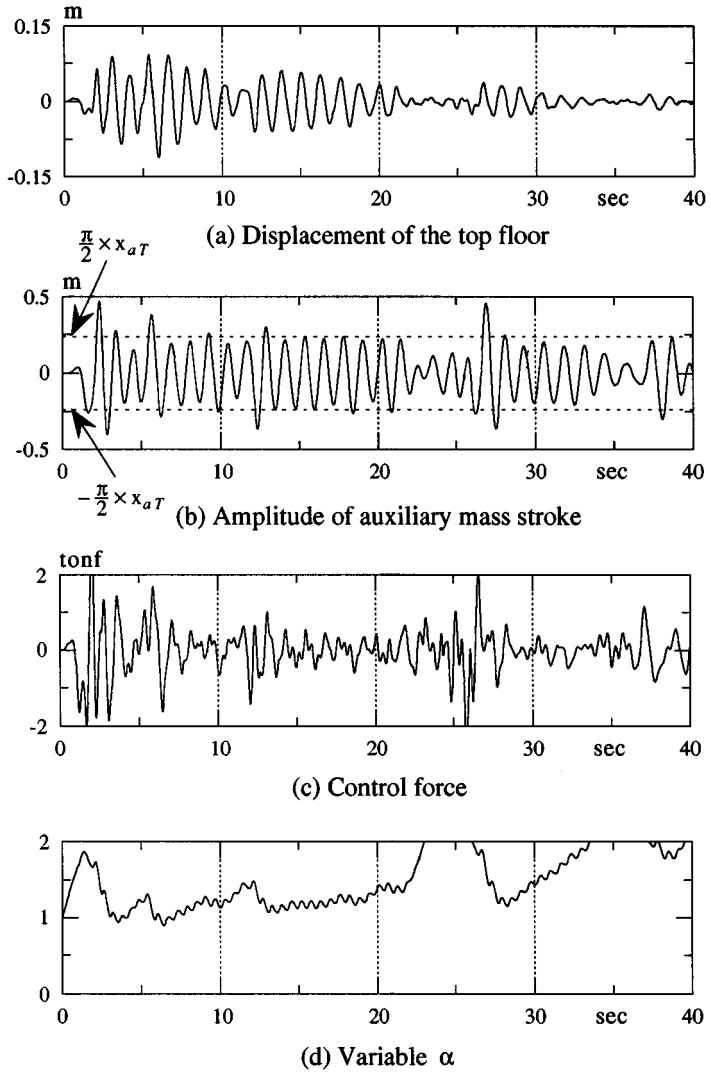

Figure 15. Time-history responses of the 10 DOF building–AMD system subjected to 1940 El-Centro NS earthquake excitation with 2·0 m/sec/sec PGA

5. CONCLUSION

The proposed control method considers the stroke length limit of the auxiliary mass, which is regarded as the principal physical constraint for application of AMD systems to actual structures. It is shown that (1) the proposed design procedure enables one to get a set of variable feedback gains that governs a trade-off between the reduction of the building response and the amplitude of the auxiliary mass stroke and (2) the proposed on-line algorithm adapts the control performance to the variation in the intensity level of sinusoidal excitations such that he amplitude of the auxiliary mass stroke attains a constant value within its limits.

A simple design method of SOF controller for modal control of buildings with non-classical damping, is also presented. An efficient control method is developed with combined use of the VGF control and the SOF control for a hybrid structural control.

It is demonstrated through numerical examples that (1) the proposed VGF control effectively adapts the control performance against both seismic and sinusoidal excitations in such a manner that the amplitude of the auxiliary mass stroke is kept within its limits, (2) due to the smooth control performance, no control chattering occurs and (3) the maximum control power is restrained as well. Finally, the capacity of the AMD system is fully utilized from weaker to stronger external excitations, and both the application range and the reliability of the AMD system are improved significantly compared to that achieved by the conventional constant gain feedback control.

It is to be noted that the proposed control method is applicable to the VGF control with the control force limit as well.

ACKNOWLEDGEMENT

The authors are most grateful to Prof. Tsuneyoshi Nakamura, Department of Architecture and Environmental Design, Kyoto University, for the support and suggestions in the course of this study. The cooperation of Mr. Shozo Nishiyama and Dr. Binod K. Bhartia in the initial stage of this research is also acknowledged. We also wish to thank Dr. Misko Cubrinovski for his review of this paper and his comments.

REFERENCES

1. J. N. Yang and T. T. Soong, 'Review paper; recent advances in active control of civil engineering structures', *Probab. eng. mech.* **3**, 179–188 (1988).
2. M. Izumi *et al*., 'Building with response control systems in Japan', in A. H. Ang and R. Villaverde (eds), *Structural Engineering in Natural Hazards Mitigation*, Vol. 1, ASCE 1993 Structures Congress, Irvine, CA, 1993, pp. 107–114.
3. T. Kobori, N. Koshika, K. Yamada and Y. Ikeda, 'Seismic-response-controlled structure with active mass driver system. Part 1: design', *Earthquake Engng. Struct. Dyn.* **20**, 133–149 (1991).
4. T. Fujita, T. Kamada, N. Masaki and Y. Suizu, 'Active mass damper using multistage rubber bearing and hydraulic actuator', *Proc 10WCEE*, Vol. 4, 1992, pp. 2073–2076.
5. K. Maebayashi, K. Shiba and Y. Inada, 'Hybrid mass damper system for response control of buildings', *Proc. 10WCEE*, Vol. 4, 1992, pp. 2359–2364.
6. M. Higashino and S. Aizawa, 'The application of active mass damper system in actual buildings', *Proc. int. workshop on structural control*, Honolulu, Hawaii, 1993, pp. 194–205.
7. J. Hirai, H. Abiru and E. Tsuji, 'Study on tuned active damper for control tower of Kansai international airport', *Proc. int. workshop on structural control*, Honolulu, Hawaii, 1993, pp. 206–213.
8. W. M. Wonham and C. D. Johnson, 'Optimal bang-bang control with quadratic performance index', *J. basic eng. trans. ASME* 107–115 (1964).
9. B. Bhartia and I. Nagashima, 'On saturation control of buildings with active mass damper', *Trans. Japan national symp. on active structural response control*, 1992, pp. 57–64.
10. B. Bhartia, Y. Fujino and J. Mongkol, 'Control algorithm for AMD with constraints', *Proc. 1st world conf. on structural control*, Los Angeles, Vol. 2, 1994, pp. TP2-70–78.
11. R. E. Kalman and J. E. Betram, 'Control system analysis and design via the "second method" of Lyapunov (I)', *J. basic eng. trans. ASME* 371–393 (1960).
12. J. M. Kelly, G. Leitmann and A. G. Soldatos, 'Robust control of base-isolated structures under earthquake excitation', *J. optim. theory applic.* **53**, 159–180 (1987).
13. B. Bhartia and I. Nagashima, 'Saturation control of buildings with AMD of bounded capacities', *Proc. 34th AIAA/ASME/ASCE/AHS/ASC structures, structural dynamics, and materials conf.*, Lajolla, CA, 1993, pp. 3561–3569.

14. B. Indrawan, T. Kobori, M. Sakamoto and N. Koshika, 'Analytical study on a new power-efficient active control method', *Proc. 2nd int. conf. on motion and vibration control*, Yokohama, 1994, pp. 687–692.
15. A. Preumont, 'Spillover alleviation for nonlinear active control of vibration', *J. guidance control* **11**, 124–130 (1988).
16. K. Yoshida, Y. Nishimura and Y. Yonezawa, 'Variable gain feedback control for linear sampled-data systems with bounded control', *Control theory adv. technol.* **2**, 313–323 (1986).
17. T. Fujita, T. Kamada and N. Masaki, 'Fundamental study of active mass damper using multistage rubber bearing and hydraulic actuator for vibration control of tall buildings: Part 1 study on control law for the active mass damper', *Trans JSME* **58**, 87–91 (1992).
18. T. Suzuki, M. Kageyama *et al.* 'Active vibration control system for high-rise buildings. Part 14: vibration test on variable feedback gain control', *Trans. AIJ annual meeting*, 1993, pp. 735–754 (in Japanese).
19. N. Kawai, M. Ohtsuka *et al.*, 'A development of active response control system. Part 3: shaking table test results on variable gain control method', *Trans. AIJ annual meeting*, 1994, pp. 895–896 (in Japanese).
20. J. P. Den Hartog, *Mechanical Vibrations*, 4th edn, McGraw-Hill, New York, 1956.
21. N. R. Draper and H. Smith, *Applied Regression Analysis*, 2nd edn, Wiley New York, 1981.
22. W. S. Levine and M. Athans, 'On the determination of the optimal constant output feedback gains for linear multivariable systems', *IEEE trans. automatic control* **AC-15**, 44–48 (1970).
23. D. D. Moerder and A. J. Calise, 'Convergence of a numerical algorithm for calculating optimal output feedback gains', *IEEE trans. automatic control* **AC-30**, 900–903 (1970).
24. L. L. Chung, C. C. Lin and S. Y. Chu, 'Optimal direct output feedback of structural control', *J. eng. mech ASCE* **119**, 2157–2173 (1993).
25. I. Nagashima and S. Nishiyama, 'Response control of buildings with active mass damper. Part 1: study on design method of output feedback controller and its performance', *J. struct. constr. eng.* AIJ (468) 27–37 (1995) (in Japanese).
26. I. Nagashima and S. Nishiyama, 'Study on control of transverse-tortional coupled vibrations of a structure with uni-axial eccentricity using active mass dampers', *J. struct. eng.* **42B**, 595–603 (1996) (in Japanese).
27. Y. Takahashi, H. Thal-larsen *et al.*, 'Mode oriented design viewpoint for linear, lumped-parameter multivariable control systems', *J. basic eng. trans. ASME Ser. D.* **90**, 222–230 (1968).
28. M. J. Balas, 'Active control of flexible system', *J. optim. theory appl.* **25**, 415–426 (1978).
29. L. Meirovitch and H. Baruh, 'The implementation of modal filters for control of structures', *J. guidance* **8**, 707–716 (1985).
30. N. Niwa, T. Kobori *et al.*, 'Passive seismic response controlled high-rise building with high damping device', *Earthquake Engng. Struct. Dyn.* **24**, 655–671 (1995).

